Investigating roughness effects on ship resistance in shallow waters

Soonseok Song[1,+], Momchil Terziev[2,+,*], Tahsin Tezdogan[3], Yigit Kemal Demirel[4], Claire De Marco Muscat-Fenech[5], Atilla Incecik[2]

[1]*Department of Naval Architecture & Ocean Engineering, College of Engineering, Inha University, South Korea.*

[2]*Department of Naval Architecture, Ocean and Marine Engineering, Henry Dyer Building, University of Strathclyde, 100 Montrose Street, Glasgow, UK.*

[3]*Department of Civil, Maritime and Environmental Engineering, University of Southampton, Southampton, UK.*

[4]*160 Bothwell Street, Glasgow, UK.*

[5]*Department of Mechanical Engineering, University of Malta, MSD2080 Msida, Malta*

[+]*These authors contributed equally to this paper and can be regarded as joint first authors.*

[*]Corresponding author: momchil.terziev@strath.ac.uk

Abstract

Shallow waters influence the behaviour and performance of a vessel by modifying the local pressure distribution, wave making, and boundary layer thickness. The boundary layer thickness is also influenced by surface roughness. No previous studies have investigated the combined effects of shallow water contributions and roughness on ship resistance. This study aims to fill this knowledge gap in the literature by using Unsteady Reynolds Averaged Navier-Stokes modelling. Results show that the total resistance coefficient increases between approximately 22% and 36% in the presence of roughness depending on the speed and depth-to-draft ratio. The numerical model used shows that pressure resistance grows at a faster pace than frictional resistance and increases its relative contribution to the total when roughness is applied, contrary to deep water cases.

Keywords: *Roughness effect; Unsteady Reynolds Averaged Navier-Stokes (URANS); Computational Fluid Dynamics (CFD); shallow water; ship resistance*

1. Introduction

When advancing in shallow water a ship interacts with the seabed, increasing the resistance and magnifying the sinkage and trim. These effects are primarily produced by the pressure gradient caused by the restricted area around the hull which the flow must pass through. However, shallow water influences the boundary layer of a hull as well. For example, in very shallow water such as when the depth-to-draft ratio is below 1.3, the boundary layer may intersect the seabed (Gourlay and Tuck, 2001; Shevchuk et al., 2016). Scale effects are also thought to be greater in shallow water than in deep water since boundary layers are caused by viscosity (Terziev et al., 2021b, 2022; Tuck, 1978). It is therefore important to consider boundary layer physics in a way that represents reality as closely as possible.

Hull roughness has been shown to increase the thickness of the boundary layer along with the total resistance of the hull considerably in deep waters leading potentially to speed loss and additional costs (Schultz et al., 2011). If, as suggested by Chillcce and Moctar (2022), trim can vary by a factor of approximately 4 when the depth-to-draft ratio is 1.2 due to viscous effects, then the presence of roughness or biofouling on a ship's hull may influence trim as well. Such epistemic uncertainties can affect optimum performance predictions and increase the risk of grounding accidents. To the best of the authors' knowledge, no existing research has investigated the effect of roughness and the relatively thicker boundary layer under shallow water conditions.

Recent research suggests that viscosity affects trim due to its effect on the pressure field around the hull, particularly when the depth-to-draft ratio is small (Chillcce and Moctar, 2022). The aim of this paper is to fill the aforementioned gap in the literature by examining the impact of hull roughness on ship performance using Computational Fluid Dynamics (CFD). Specifically, the effect of surface roughness on ship hydrodynamics in calm, shallow water was studied. The commercially available Reynolds Averaged Navier-Stokes (RANS) solver, Star-CCM+, version 16.04.008-r8, was used to conduct all investigations presented in this paper.

The remainder of this paper is organised as follows. Section 2 contains background pertaining to biofouling and shallow water ship performance investigations using CFD, while Section 3 explains the rationale behind the case study selection. Section 4 gives the numerical set up details. Then, Section 5 presents the results and discussion. Finally, conclusions and recommendations for future work are given in Section 6.

2. Background

A ship advancing in shallow water experiences a hydrodynamic interaction with the seabed causing changes in performance and attitude relative to deep water. The

restricted available space between the hull and seabed, or equivalently, blockage, causes water to flow differently when compared to unrestricted waters. Following Bernoulli's principle, the flow must accelerate when passing around the vessel (Lataire et al., 2012). Consequently, the pressure and water level must drop, causing an increase in the running sinkage and trim (Chen, 2013). Resistance is also affected by the proximity of the seabed in a highly complex fashion.

Depending on the depth Froude number ($F_h = U/\sqrt{gh}$, the ratio of ship speed, V, and wave speed, $\sqrt{gh}$), the resistance may increase or decrease with increasing speed unlike in unrestricted waters (Benham et al., 2020). For example, waves consume more energy in shallow water meaning that wave resistance is of greater importance than in deep water (Havelock, 1921; Inui, 1954). Recent research has demonstrated that friction is also magnified (Zeng et al., 2019a, 2019b). The mechanism by which this occurs is highly dependent on the hull form raising questions for the accuracy of the universally applied expressions (Zeng et al., 2018).

Changes in resistance, particularly in terms of friction resistance suggest changes in the boundary layer of the ship. Gourlay (2006) predicted that a vessel's boundary layer may intersect the seabed in very shallow conditions. That observation, along with numerical evidence (Shevchuk et al., 2016) of boundary layer formation on the seabed in very shallow conditions have motivated the present study. In addition, many studies have shown that ship boundary layers thicken considerably when roughness or biofouling is introduced (Song et al., 2020b). Yet, no existing research has documented the effects of fouling on resistance, sinkage, or trim in shallow waters. The present study aims to fill this gap in the literature. The remainder of this section reviews literature on fouling and roughness modelling using CFD, and ship squat prediction in shallow waters. A review and comparison of fouling modelling approaches as they apply to ship CFD is given by Andersson et al. (2020).

Demirel et al. (2014) developed a modified wall-function approach for CFD predictions of the added hydrodynamic resistance due to surface roughness, employing the Colebrook-type roughness function of Grigson (1992) to estimate the performance of antifouling coatings. The results of Demirel et al. (2014) agreed well with the experimentally-obtained results of Schultz (2004). Later, Demirel et al. (2017a) proposed a new roughness modelling approach in CFD using experimental data from Schultz and Flack (2007).

Recent studies of surface roughness effects on ship hydrodynamics have focused on practical applications (Seok and Park, 2020). For example, Song et al. (2019) demonstrated that a fouled ship surface has a measurably thicker boundary layer compared to a smooth surface using a validated model (Song et al., 2020a). The type

of fouling determines the magnitude of the increase in resistance (Demirel et al., 2017b). For example, biofilm (Farkas et al., 2018) can reduce the speed of a ship by approximately 8.5% (Farkas et al., 2020b). Experimental (Song et al., 2021) and numerical evidence (Ravenna et al., 2022) have shown that the location of the roughness is also highly influential on the resistance increase.

García et al. (2020) tested fouling resistant coatings experimentally and modelled the resulting increase in drag using OpenFOAM. The study of García et al. (2020) showed that a prediction of the change in frictional resistance alone is insufficient to determine the change in the total drag since fouling influences the pressure resistance of a hull. If marine biofouling is allowed to accumulate, resistance may effectively double (Regitasyali et al., 2021). However, incorporating the effect of surface roughness may also lead to enhanced predictive accuracy relative sea trials, as shown by Mikkelsen and Walther (2020). The aforementioned research investigated the resistance of a ship in deep, unrestricted waters. To the best of the authors' knowledge, there is no existing literature on the shallow water effect combined with hull roughness.

As has been demonstrated above for roughness, ship squat can also be predicted through numerical and experimental methods. Current scientific consensus is that viscous effects contribute little if at all to ship squat, as evidenced by the successes of potential flow-based approaches in accurately predicting the magnitude and direction of sinkage and trim of a ship in shallow water conditions (Mctaggart, 2018; Mucha et al., 2016). In fact, Mucha and el Moctar (2014) compared potential flow-based methods with RANS-based methods and found that in certain cases, the former can outperform the latter. Terziev et al. (2018) compared numerical solutions with the well-known slender body theory (Beck et al., 1975; Gourlay, 2014, 2008; Gourlay et al., 2015; Tuck, 1967, 1966) finding that as viscous contributions are the cause of a divergence in the predicted results at high speeds.

As mentioned in the introduction, recent work by Chillcce and Moctar (2022) predicted a considerable viscous effect on trim by comparing Euler and RANS simulations under otherwise identical conditions. Other studies employing the RANS method include Bechthold and Kastens (2020) who found that sinkage and resistance may be predicted robustly and consistently, but trim is more difficult to quantify. Similar findings can be interpreted through the work of Terziev et al. (2020a), who predicted an average error in resistance of less than 5% across 8 different eddy-viscosity turbulence models, such as the realisable κ-ε, standard κ-ω, and κ-ω *SST* models. Elsherbiny et al. (2019) modelled the KRISO container ship (KCS) in different canals using CFD, finding good agreement with experimental results across their case studies.

3. Case studies

For the purposes of the present study, case studies featuring shallow to very shallow conditions are necessary to gauge the effects of roughness on ship hydrodynamics. It is known that beyond a depth-to-draft ratio (h/T) of about 2.5, shallow water effects become insignificant, whereas organisations such as PIANC (2014) typically define shallow and very shallow conditions when $h/T < 1.5$. Although these factors limit the number of experiments available to compare numerical models against, several possibilities remain for the chosen hull form, the KRISO container ship (KCS). Specifically, Mucha and el Moctar (2014) presented experimental data for the KCS when the depth-to-draft ratio is 1.3. The resistance data from that experiment are used to compare the performance of the numerical model.

The principal characteristics of the KCS, as modelled experimentally by Mucha and el Moctar (2014) are given in Table 1. It should be noted that unlike the design loading condition, correspoding to a full-scale draft of 10.8m, the aforementioned experimental campaign used a draft of 10m instead.

Table 1. Principal characteristics of the KCS (Mucha and el Moctar, 2014).

Property	**Symbol**	**Full-scale value**	**Model-scale value**	**Units**
Scale factor	λ	1	40	-
Length	L	229.2	5.73	m
Beam	B	32.2	0.805	m
Draft	T	10	0.25	m
Block coefficient	C_B	0.64	0.64	-
Wetted surface area	S_w	8992	5.62	m^2

In addition to the case study presented by Mucha and el Moctar (2014) where h/T =1.3, the present study modelled h/T =1.1 and 1.2 to gauge the effect of different water depths. One of the selected velocities used by Mucha and el Moctar (2014), U =0.73m/s, corresponding to a depth Froude number of F_h =0.409 and 9kn in full-scale. That speed was supplemented by U =0.6m/s and 0.5m/s, which correspond to approximately 7.4kn and 6.15kn, respectively. The full test matrix is given in Table 2. It should be noted that all case studies presented herein were carried out in model-scale (λ=40).

Table 2. Test matrix (values given in model-scale, λ=40).

Case study number	**U (m/s)**	**F_h**	**h/T**	**Depth (m)**
1	0.5	0.304	1.1	0.275
2	0.6	0.365		
3	0.73	0.444		
4	0.5	0.292	1.2	0.3

5	0.6	0.35		
6	0.73	0.426		
7	0.5	0.28	1.3	0.325
8	0.6	0.336		
9	0.73	0.409		

4. Numerical set up

The commercially available RANS solver, Star-CCM+ version 16.06.10-r8 was used for all numerical modelling. The solver utilises the Finite Volume method to discretise the domain into a finite number of adjoining cells. The computational domain arrangement follows the established norms by the ITTC (2014). Namely, the inlet which introduces the flow in the negative x direction using a velocity inlet boundary condition is placed 1.5 ship lengths upstream of the forward perpendicular. The outlet is placed 2.5 ship lengths downstream of the aft perpendicular with a pressure outlet which maintains the hydrostatic pressure and prevents backflow. A symmetry plane is placed coincident with the canal and ship centreline.

To accelerate convergence of the solution, wave damping is applied in the normal direction to the inlet and outlet boundaries over a distance of 1 ship length. The domain top, a velocity inlet, is placed approximately one ship length from the undisturbed waterline. The domain bottom and side are positioned according to the case studies shown in Table 2, where a no-slip boundary condition is applied. In addition, a relative velocity equal but opposite to the ship velocity is assigned to the bottom and side boundaries. Doing so ensures there is no relative motion between the seabed and side relative to the flow when it is introduced in the domain. In the ship's frame of reference, the flow, bottom, and side move downstream at the same velocity. The computational domain is depicted in Figure 1.

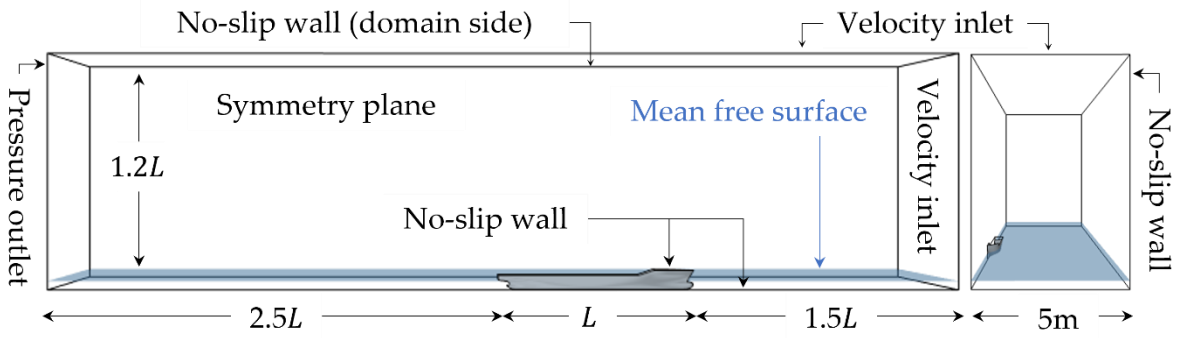

Figure 1. Graphical depiction of the computational domain and applied boundary conditions. Depicted: h/T =1.1.

The ship's sinkage and trim are modelled through mesh morphing. That is, the grid is deformed to achieve the equilibrium position of the vessel. The motion in the $x-z$

plane is modelled through the Dynamic Fluid-Body Interaction (DFBI) module of Star-CCM+. The hull is prevented from moving during the first 5 seconds of simulation time to avoid large-amplitude motions induced by the impulsive start of the flow. The hydrodynamic forces are then gradually applied over a further 5 seconds of physical time. All simulations are run for a minimum of 300s to ensure adequate convergence of results.

4.1 Near-wall grid

The near-wall grid set-up is of critical importance when modelling roughness. Following precedent from earlier studies on roughness effects on ship hydrodynamics (Demirel et al., 2017a, 2017b, 2014; Farkas et al., 2020a, 2020b; Song et al., 2021, 2019), the *k-ω* SST turbulence model is used throughout (Menter, 1994) with a high y^+ wall treatment on the hull.

The distribution and size of near-wall layers on the hull is known *a priori* by using the methodology shown in Terziev et al. (2022) and used in Terziev et al., (2021). Namely, the distance over which near-wall layers are distributed is expressed as the sum of a geometric series whose common ratio (S) is the expansion factor between two adjacent cells, and the series' first element is the first cell thickness ($2\Delta y$).

The procedure begins by expressing the skin friction coefficient through the ITTC correlation line:

$$C_F = 0.075/(\log_{10} Re - 2)^2 \quad (1)$$

where $Re = LV\rho/\mu$ is the Reynolds number, $\rho = 997.561\text{kg/m}^3$ is the fresh water density, and $\mu = 8.8871\times10^{-4}$ Pa-s is the dynamic viscosity. The local shear stress can be found using $\tau_w = C_f \rho V^2/2$. Once these parameters are known alongside the desired y^+ value, the first layer half-thickness is $\Delta y = y^+ v/u_t$ with $U_\tau = \sqrt{\tau_w/\rho}$ being the friction velocity and $v = \mu/\rho$ the kinematic viscosity (Peric, 2019). The total number of layers, n, is found by using Eq. (2):

$$n = \log\left(1 - \frac{\delta(1-S)}{2\Delta y}\right) / \log(S) \quad (2)$$

where δ is the distance over which layers are to be distributed. It should be noted that approach explained above is approximate since curvature and local flow acceleration are not considered. The y^+ value will be influenced near the seabed in particular where the flow must accelerate significantly due to the proximity of the seabed, causing the y^+ values to be higher there. Conversely, near the high-pressure areas of the bow and stern, the flow will decelerate, causing the y^+ value to reduce. Choosing a high y^+ mesh reduces the overall cell numbers while ensuring that the accelerated flow does not cause the local y^+ values to enter the buffer layer ($5 > y^+ > 30$). All

simulations presented in this paper use $\delta \approx 0.0233$ m, $S = 1.35$, and n =3. With these settings, a y^+ ≈53 is achieved when h/T =1.1, U =0.5 m/s, where the above method predicts y^+ ≈67.3 under ideal conditions (no surface curvature, external velocity gradients, etc), highlighting the importance of allowing for the shallow water effect on the y^+. For example, when the water depth corresponds to h/T =1.3 and $U = 0.5$ m/s, the achieved y^+ is 67.9, showing the capability of the method. It should be noted that the y^+ values on the seabed are maintained below $y^+ = 1$.

4.1 Roughness effect modelling

The aim of this subsection is to introduce the numerical approach to modelling roughness and its impact on the flow. That impact can be seen as a downward shift in the turbulent boundary layer's velocity profile. This downward shift is termed as the *roughness function*, ΔU^+. The non-dimensional velocity profile in the log-law region for a rough surface is then given as:

$$U^+ = \frac{1}{\kappa}\ln y^+ + B - \Delta U^+ \tag{3}$$

where U is the mean velocity at the normal distance, y, from the wall, and κ is the von Karman constant and B is the log law intercept.

The roughness function, ΔU^+ can be written as a function of the roughness Reynolds number, k^+, defined as:

$$k^+ = kU_\tau/\nu \tag{4}$$

in which, k is the roughness height of the surface. It is of note that ΔU^+simply vanishes in the case of a smooth wall. Once the roughness function model ($\Delta U^+ = f(k^+)$) of the surface is known, the modified wall-function (Eq. 3) can be used in CFD simulations to simulate the flow over the rough surface.

Song et al. (2021) conducted towing tests with a flat plate coated with 60/80 grit aluminium oxide abrasive powder and determined the roughness function of the rough surface. Around the same time, Song et al. (2020) proposed a mathematical model of the roughness function (i.e. roughness function model) to model the rough surface in CFD simulations with the modified wall-function approach. As proposed by Song et al. (2020), the roughness function model for the 60/80 grit sand grain surface can be written as:

$$\Delta U^+ = \begin{cases} 0 & \rightarrow \quad k^+ < 3 \\ \frac{1}{\kappa}\ln\left(0.49k^+ - 3\left(\frac{k^+-3}{25-3}\right)\right)^{\sin\left[\frac{\pi}{2}\frac{\log(k^+/3)}{\log(25/3)}\right]} & \rightarrow \quad 3 \le k^+ < 25 \\ \frac{1}{\kappa}\ln(0.49k^+ - 3) & \rightarrow \quad 25 \le k^+ \end{cases} \tag{5}$$

in which, k^+ is the roughness function obtained based on the maximum peak to trough roughness height over a 50 mm interval (i.e. $k = Rt_{50} = 353$ μm). As shown in Figure 2, the roughness function model of Song et al. (2020) shows an excellent agreement with the experimental roughness function of Song et al. (2021).

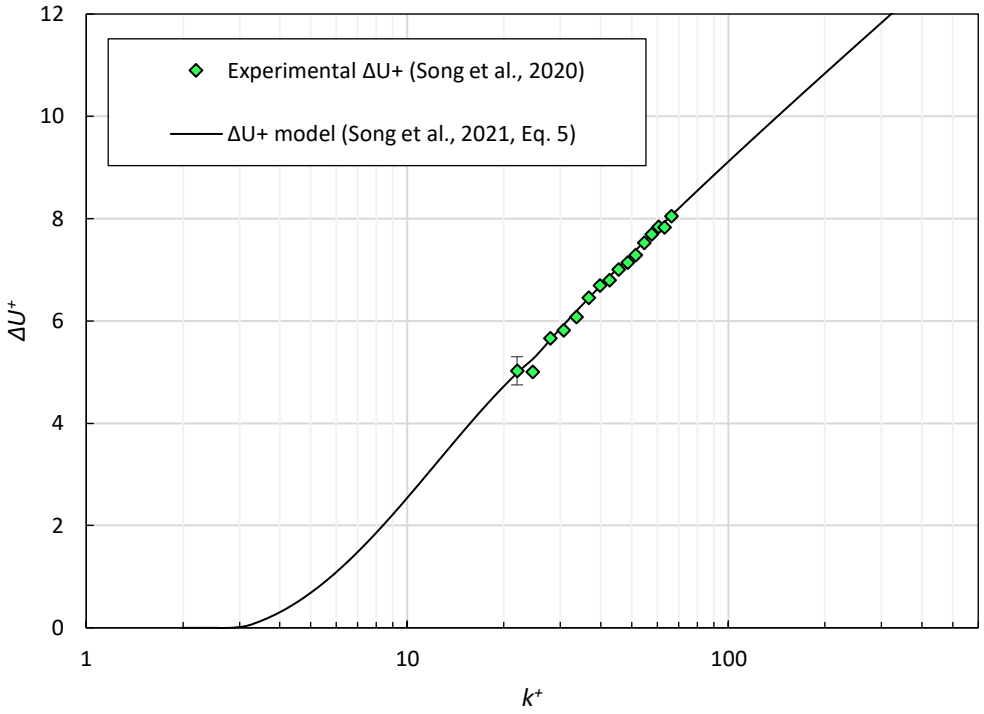

Figure 2. Experimental roughness function Song et al. (2021) and the roughness function model of Song et al. (2020) (Eq. 5).

Song et al. (2020) modelled CFD simulations of the towed flat plate and KCS model and validated the modified wall-function approach and the roughness function model (Eq. 5) by comparing the results with the experimental data of Song et al. (2021).

4.2 Mesh generation

The computational mesh is generated using the automatic facilities available within Star-CCM+. Hexahedral cells are used throughout, aligned with the main flow features. Specifically, the mesh is refined in the zone where the free surface is expected to deform and within the Kelvin wedge. The resulting mesh, containing approximately 1.2 million cells is depicted in Figure 3 and Figure 4. In shallow water, the Kelvin half-angle can increase theoretically to up to 90° (Havelock, 1908; Johnson, 1957). The selected case studies limit the Kelvin half-angle to the deep water limit of approximately 19.47° because the depth Froude numbers selected are below 0.45 (Caplier et al., 2016; Terziev et al., 2020).

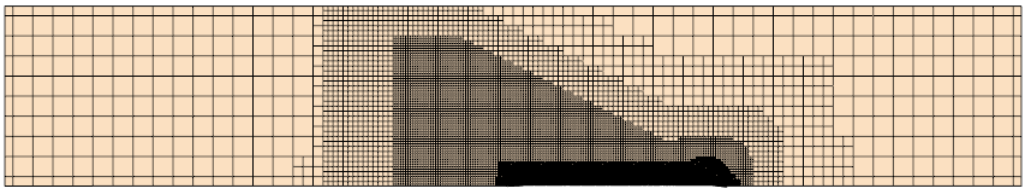

Figure 3. Top view of the generated mesh on the water surface.

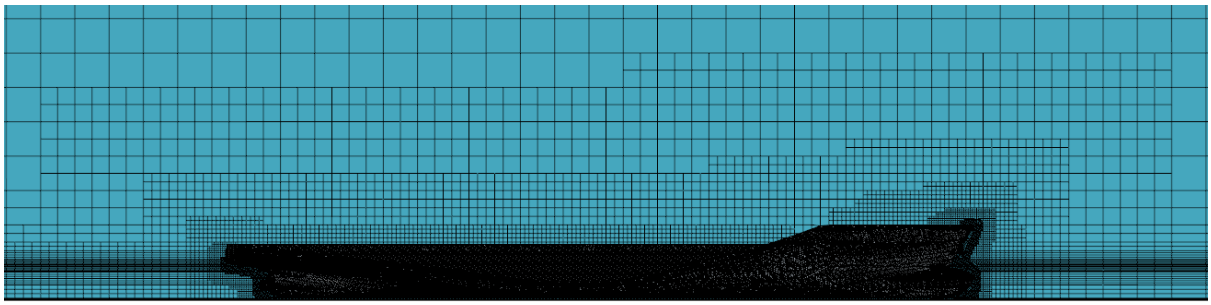

Figure 4. Close-up side view of the generated mesh on the symmetry plane and the hull. Depicted: h/T =1.1.

4.3 Time step selection

The recommendations for selecting the time step used by Terziev et al. (2018) are followed of $\Delta t = 0.0035 L/U$. It should be noted that the adopted time step value is smaller than the recommendations of the ITTC, $\Delta t = 0.005 \sim 0.01\ L/U$. Recently, the efficacy of this method of setting the time step was demonstrated by Campbell et al., (2022) who validated their shallow water resistance predictions against experimental data while employing the aforementioned time stepping strategy.

5. Results and discussion

The first item to be examined in the current section is the performance of the numerical model relative to the experimental data given in Mucha and el Moctar (2014). A comparison of case 9 ($U = 0.73$ m/s, h/T =1.3, as shown Table 2) in Table 3, which shows the total resistance value is predicted with an accuracy of 0.97%. Sinkage and trim are considerably harder to accurately predict using CFD, as demonstrated by Bechthold and Kastens (2020) particularly when the trim attains a very small value. The sinkage is predicted with an error of 2.11%, while the trim varies by approximately one order of magnitude. It should be noted that a similar level of accuracy was achieved by Mucha and el Moctar (2014) for the same case study as well as Terziev et al. (2019). Due to the small relative difference in the obtained results, the level of agreement is deemed adequate.

Table 3. Comparison between experimental results, EFD, given in Mucha and el Moctar (2014) and numerical results obtain in this study (CFD).

Property	**EFD**	**CFD**	**Units**
Total resistance	8.317	8.236	N
Sinkage	6.160	6.290	mm
Trim	-0.0224	-0.0012	°

Next, it is useful to examine the discretisation uncertainty of the numerical model using the Grid Convergence Index (GCI). The GCI procedure requires a grid triplet, obtained by systematically coarsening the fine solution (Celik et al., 2008). Following recommendations by Burmester et al. (2020) the Courant number is kept the same during the GCI procedure by simultaneously varying the grid dimension and time step by the same factor. As suggested by ITTC (2008) and ASME (American Society of Mechanical Engineers, 2009), that factor, known as the grid refinement factor is chosen as $r = \sqrt{2}$.

A systematic coarsening of the grid twice yields the fine (f_1), medium (f_2), and coarse (f_3) solutions consisting of approximately 1.2 million, 0.69 million, and 0.4 million cells, respectively. Once these three simulations are ran, one can obtain the difference between the medium – fine solutions (ε_{21}) and coarse – medium solutions (ε_{32}). The values of ε_{21} and ε_{32} are used to obtain the order of accuracy:

$$p = \ln(\varepsilon_{32}/\varepsilon_{21})/\ln r \tag{6}$$

which is used to predict the GCI uncertainty:

$$GCI = 100 \times 1.25\varepsilon_{21}/(f_1 r^p - f_1) \tag{7}$$

The factor 1.25 is known as the Factor of Safety (Roache, 2016). The results from the GCI procedure are given in Table 4.

Table 4. Discretisation uncertainty assessment results.

Parameter	**Value**	**Units**
Fine solution (f_1)	8.24	N
Medium solution (f_2)	8.37	N
Coarse solution (f_3)	8.69	N
Order of accuracy (p)	2.24	-
GCI (%)	0.31%	-

Table 4 shows that resistance converges monotonically, with an order of accuracy of p =2.24, which is marginally higher than the theoretical order of convergence p_t =2. The corresponding GCI uncertainty is 0.31%. Such performance is deemed acceptable.

5.1 Resistance coefficients

The aim of this section is to present the resistance coefficients for all case studies given in Table 2. Total resistance is broken down its frictional component, C_F, and its pressure component, C_P. It should be noted that the pressure component contains viscous pressure resistance and wave resistance, that is, viscous and inviscid contributions. C_F and C_P represent the tangential and normal components of the force acting on the hull, respectively. The measured force in both cases is divided by $0.5\rho S_w U^2$ to convert it into its dimensionless form. A comparison between the rough and smooth coefficients obtained for all case studies are presented in Figure 5.

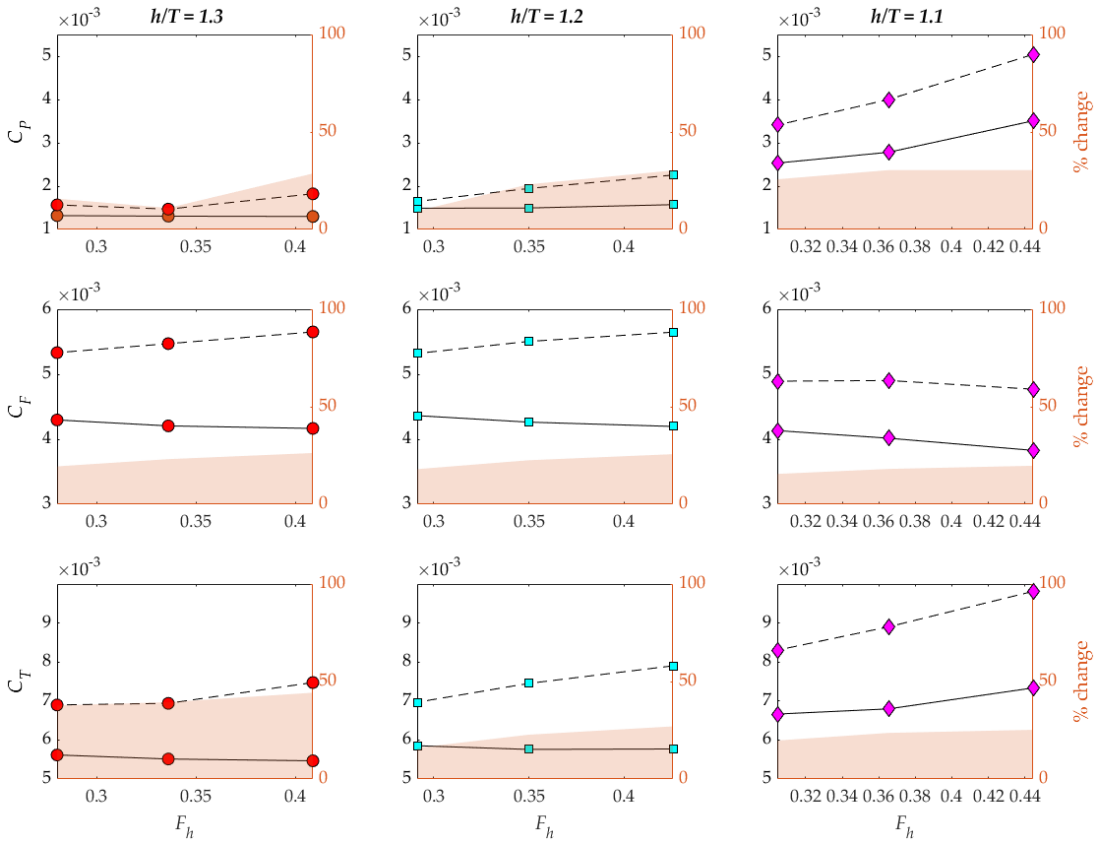

Figure 5. Comparison of resistance coefficients obtained for a smooth (solid lines) and rough (dashed lines) hull. The axes on the right show the relative change in resistance coefficient.

The resistance coefficients shown in Figure 5 indicate considerable sensitivity to the roughness. For water depths corresponding to h/T= 1.3 and 1.2, the frictional resistance dominates the increase in total resistance. However, when the KCS sails in very shallow waters corresponding to h/T =1.1, the pressure resistance increase also contributes significantly to the total resistance. These findings indicate that the magnitude of the resistance coefficient when the hull is smooth determines the relative magnitude of the increase due to roughness. That is, at low speeds and in waters that are not extremely shallow, friction will dominate the total resistance and its increase will eclipse any changes in pressure resistance due to roughness. However, as the

wave component of the pressure resistance increases due to the reduced water depth, the magnitude of change due to pressure resistance also increases.

The contribution of each resistance component to the total resistance is depicted in Figure 6, where the aforementioned effect is clearly visible. As shown in Figure 5, the relative increase in resistance coefficient is significant for all case studies. When h/T=1.1, the resulting total resistance increase ranges between 24.6% and 33.7% depending on the speed. On the other hand, when h/T=1.3, the increase in total resistance coefficient due to roughness ranges between 22.8% and 36.7%. Figure 6 shows that these increases in total resistance coefficient are strongly influenced by the speed and to a lesser extent, the water depth.

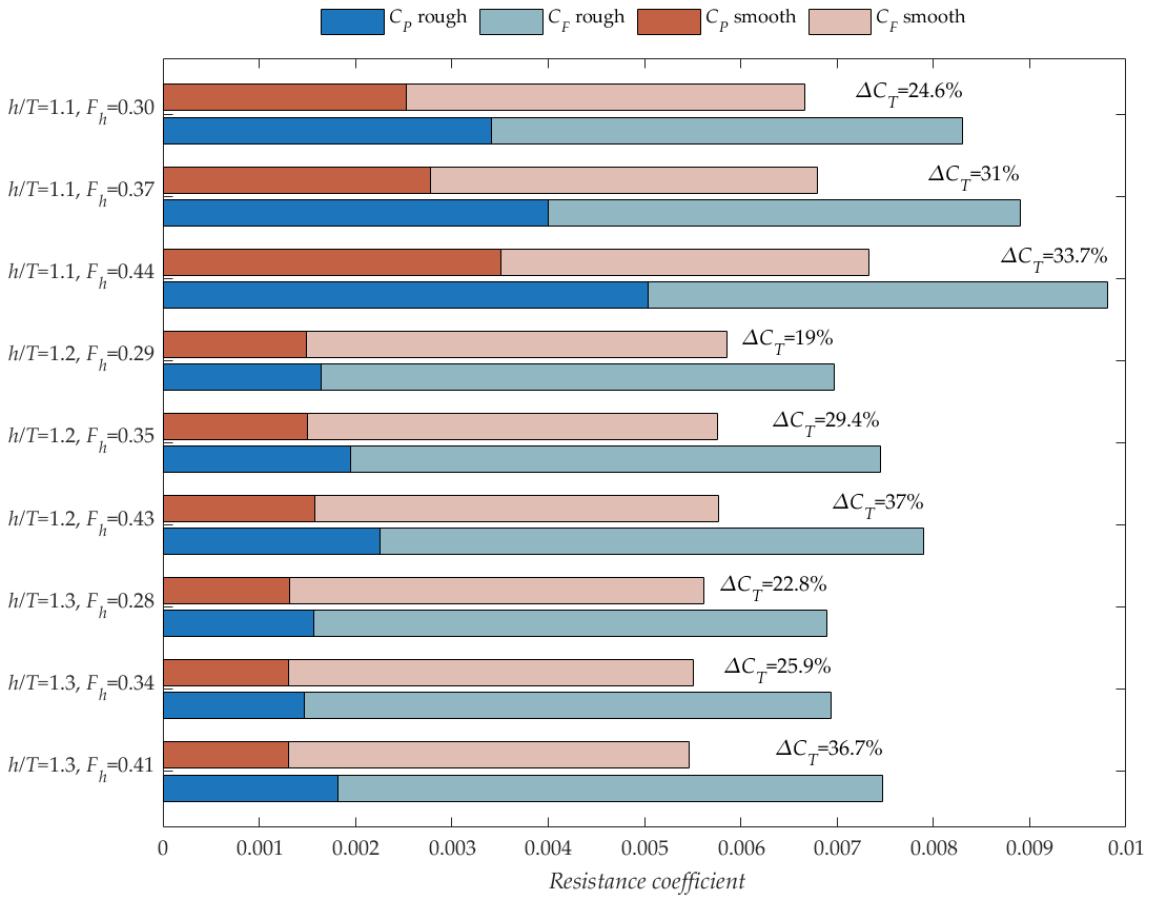

Figure 6. Total resistance coefficients and relative change due to roughness for all case studies.

Although water depth has a limited effect on the total resistance increase due to roughness, it has a considerable impact on its make-up. Figure 7 demonstrates that pressure resistance accounts for approximately 24% when h/T =1.3 and the hull is smooth. The contribution of C_P grows faster than the frictional resistance in that case under rough conditions, taking up a greater share of the total resistance by approximately 1%. On the other hand, when the conditions are very shallow and

h/T=1.1, the pressure resistance grows in importance three times faster, increasing its contribution to the total resistance by approximately 3% across all speeds. For h/T=1.1 and F_h=0.44, that increase results in the pressure resistance coefficient making up more than half of the total resistance.

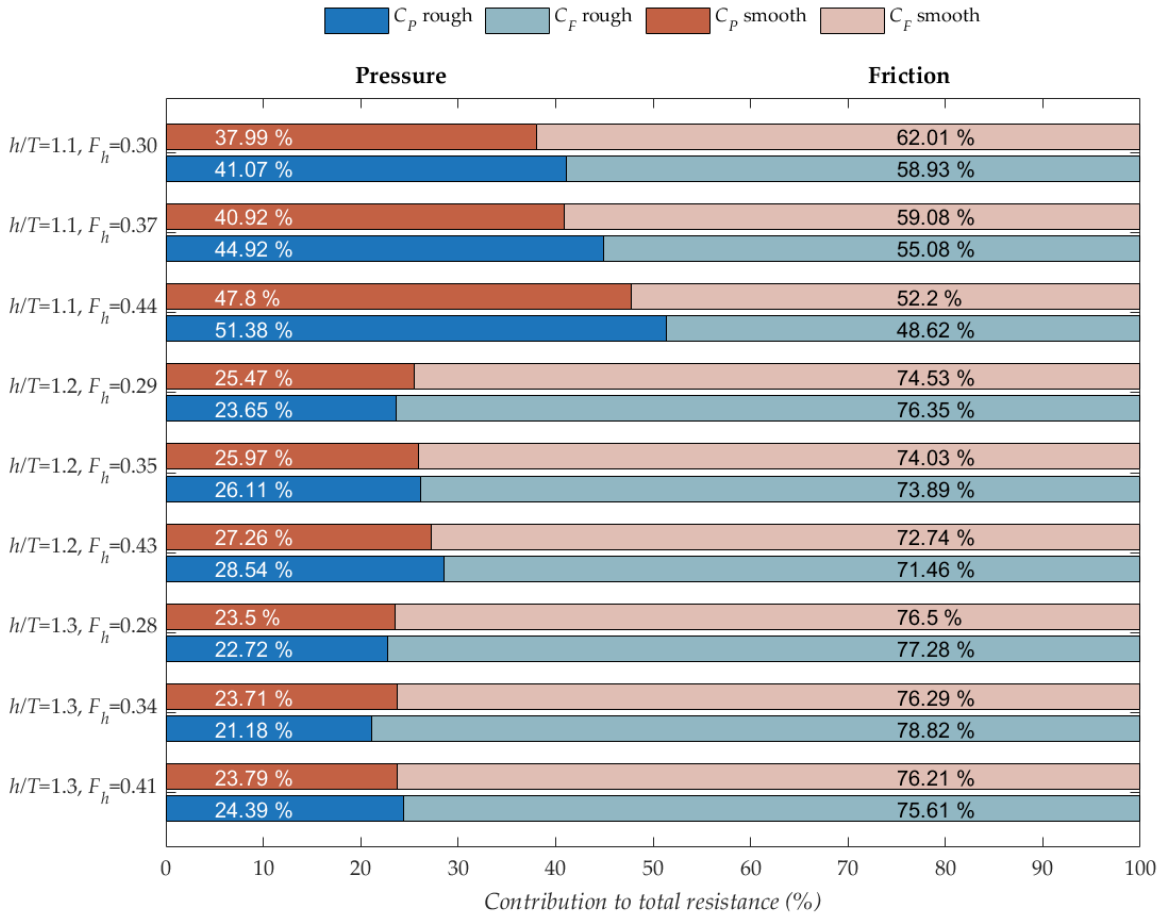

Figure 7. Make-up of the total resistance coefficient for all case studies.

The aforementioned findings have implication for resistance optimisation in shallow waters. As discussed by Campbell et al. (2022), there are several avenues one may pursue in optimising ship resistance in shallow water. The preferred approach is presently relying on potential flow-based methods, which accounts for the wave resistance of a hull only. The results depicted in Figure 6 and Figure 7 vindicate this approach, since the pressure resistance grows in importance not only with speed and depth, but also due to surface roughness. However, care should be taken in relying on purely inviscid methods since they are by definition unable to model the large increase in the magnitude of the pressure resistance coefficient. These findings also demonstrate the importance of estimating ship resistance under conditions that are as realistic as possible.

5.2 Sinkage and trim

As discussed in the introduction, one of the main aims of the present paper is to investigate if sinkage and trim vary due to roughness. This section presents the results obtained for sinkage and trim under smooth and rough hull conditions.

The sinkage results are given in Figure 8, which show that sinkage is essentially independent of roughness. Since roughness is known to affect the thickness of the boundary layer, one may expect that the vertical force acting on the hull as a result will also be affected. Our results show that such effects are minimal, and completely eclipsed by changes in sinkage due to a variation in the speed. From the point of view of sinkage, therefore, ship operators and designers can disregard the effect of surface roughness, given that the additional weight due to the accumulation of marine organisms is accounted for.

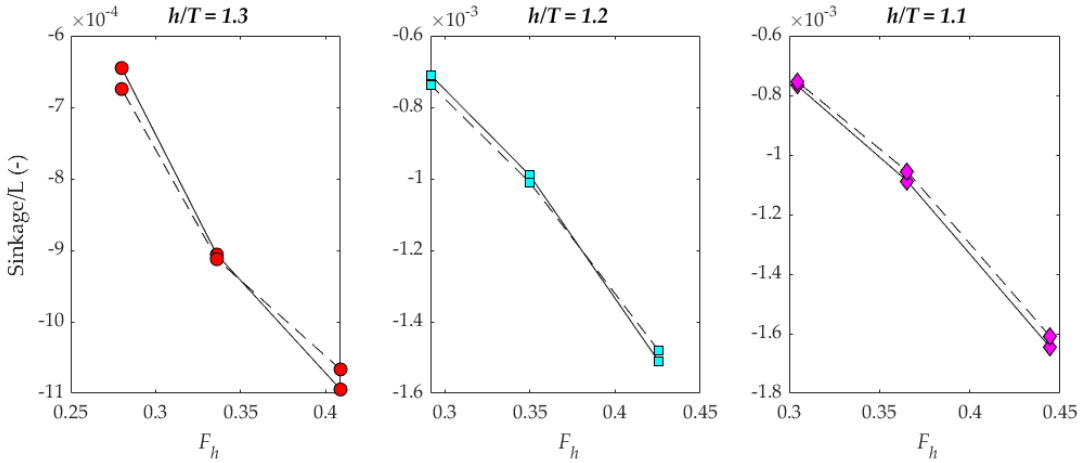

Figure 8. Sinkage results for smooth (solid lines) and rough (dashed lines) hull conditions.

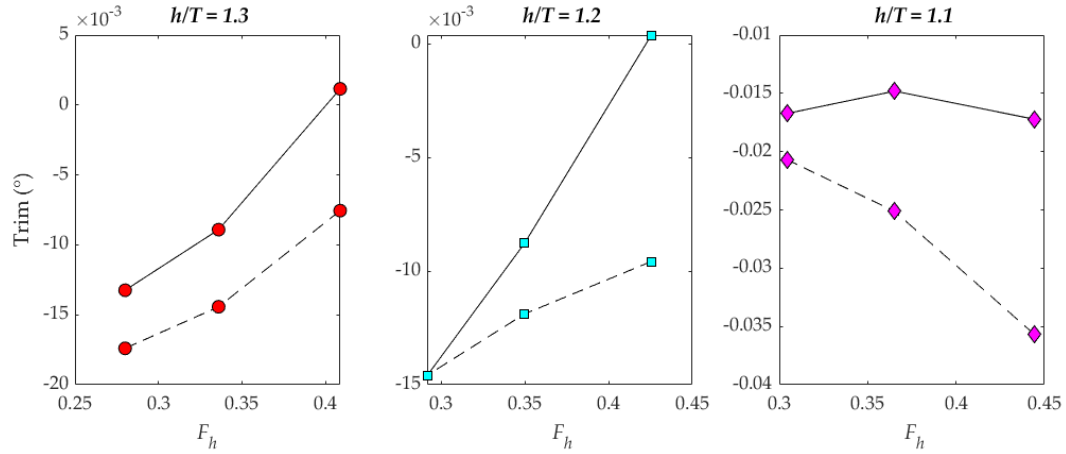

Figure 9. Trim results for smooth (solid lines) and rough (dashed lines) hull conditions.

Figure 9 depicts the results obtained for trim. It is important to recall that our numerical model did not predict trim with the same fidelity as sinkage. Nevertheless,

the CFD model shows considerable sensitivity of trim to roughness, which is in agreement with the results of Chillcce and Moctar (2022) indicating viscous effects are important in determining the magnitude of trim. These changes increase at higher speeds as well as with decreasing water depth. In all cases, roughness increases the magnitude of trim, meaning that overall ship squat attains a higher value. It is therefore important to consider the effect of hull roughness in shallow waters. However, it should be kept in mind that uncertainties in trim and sinkage and typically higher than in resistance. The relatively small magnitude of the parameters makes them notoriously difficult to predict with good accuracy.

5.3 Local flow

As discussed previously, surface roughness thickens the boundary layer of a vessel. The thickening will also change with distance from the bow and be influenced by the presence of the seabed. A boundary layer that varies in thickness over the length of a hull considerably implies a displacement thickness that is different to that of the smooth hull. These effects magnify viscous contributions to ship performance (Terziev et al., 2022). More importantly the displacement thickness will be considerably thicker at the aft than at the bow. In other words, we can take the approach adopted by the potential flow researchers in which the hull size is increased by the displacement thickness (Lazauskas, 2009). Under that framework, the resulting hull shape changes from bow to stern leading to a modified moment acting on the hull which ultimately affects trim.

The change in boundary layer thickness is exemplified in Figure 10, which compares the boundary layer of the hull under smooth and rough conditions. Figure 10 shows the velocity distribution at the aft perpendicular of the hull for all cases. As expected, the predicted stern wake for the rough hull is always greater than the smooth hull, regardless of speed or water depth. It is important to note that the extent of the difference becomes clearer as the ship speed increases, which can be explained by the increased roughness Reynolds number, k^+, (i.e. increased roughness effect) due to the higher flow speed over the hull surface. Similarly, the difference in the stern wake between the smooth and rough cases are more evident for shallower water depths, where local flow accelerations are greater due to the blockage effect.

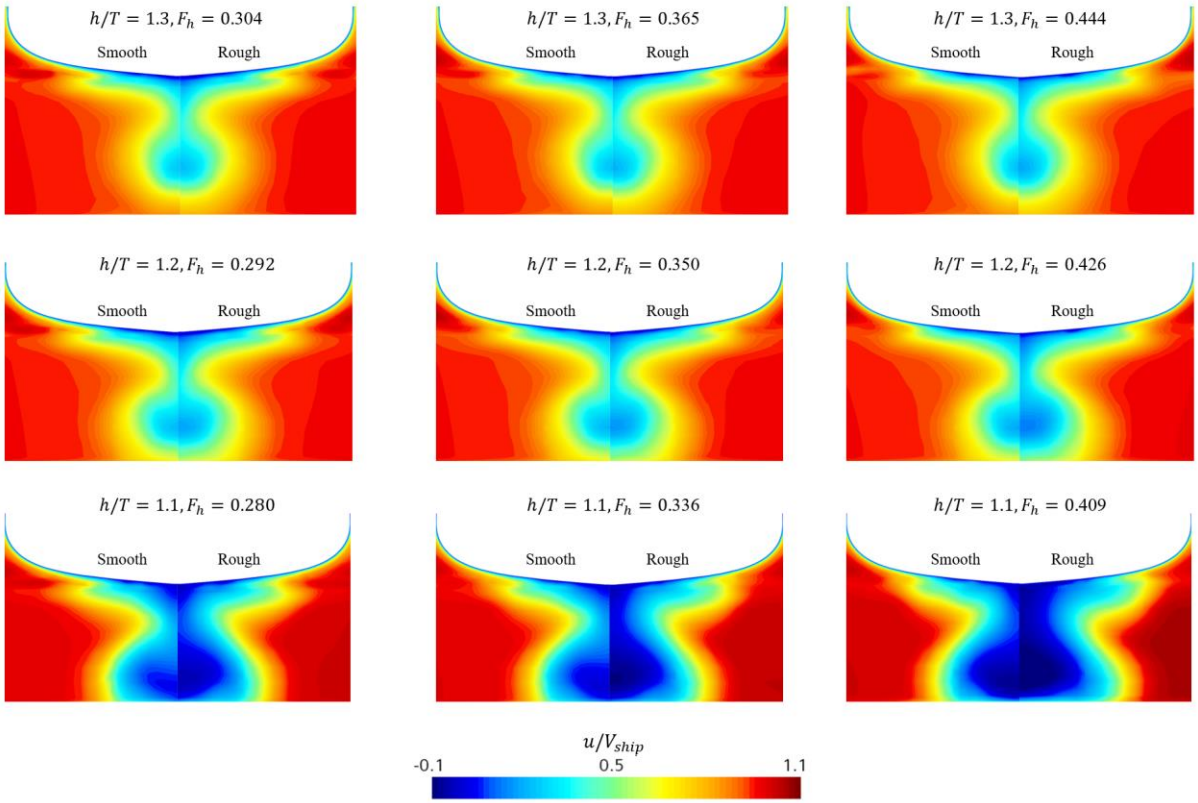

Figure 10. Wake at the aft perpendicular for all cases

The low-speed cases examined herein are dominated by the near-field disturbance. Therefore, the high-speed examples ($U = 0.73$m/s) are shown in Figure 11. While differences in the wave field are detectable when one examines the smooth and rough case of each depth-to-draft ratio presented in Figure 11, it should be kept in mind that significant variations in trim were predicted. Thus, it is not straightforward to attribute changes in the wave field solely to the inclusion of roughness.

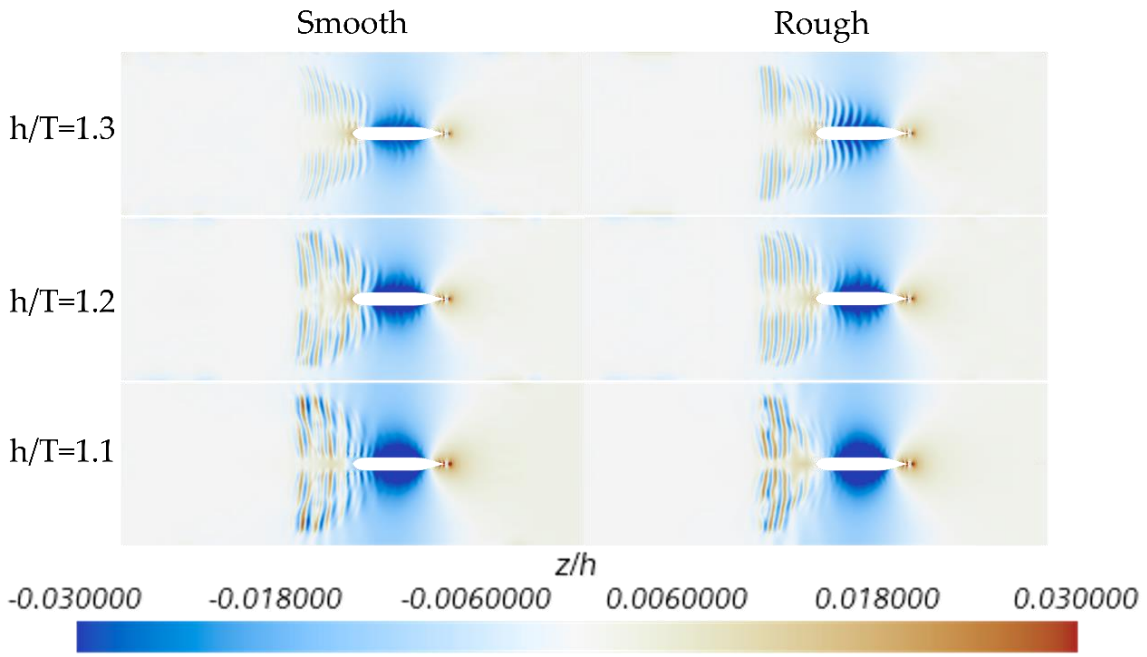

Figure 11. Wave fields produced by the hull when $U = 0.73$m/s.

Figure 12 shows the distribution of the hydrodynamic pressure coefficients (i.e. $C_{hp} = (p - \rho gh)/(½\rho V_{ship}^2)$ on the smooth and rough hulls with different speeds (i.e. F_h) and depths (i.e. h/T). Regardless of the speed and depth, all cases show decreases in the hydrodynamic pressure at the stern with the presence of hull roughness (i.e. smaller pressure recovery at the stern). These decreases in the pressure recovery can be correlated with the increased stern trim with the hull roughness shown in Figure 9. In other words, the lower stern pressure with the hull roughness resulted in smaller stern buoyancy and thus increased stern trim (i.e. stern-down). It is of note that the decreases in the pressure recovery at the stern can be attributed to the increased boundary layer thickness due to the hull roughness as similarly found in previous studies (Song et al., 2020b).

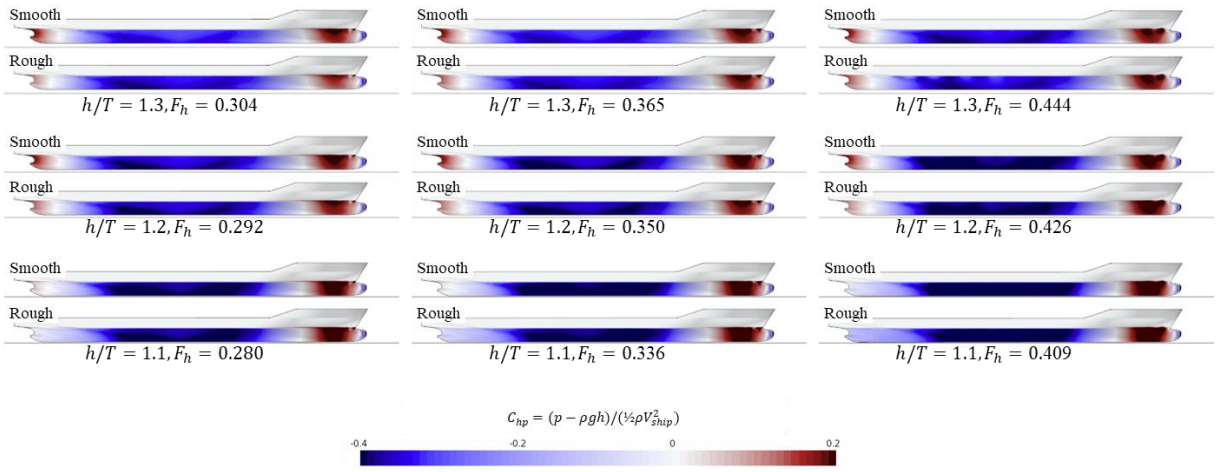

Figure 12. Hydrodynamic pressure on the hull surface

6. Conclusion and recommendations for future work

The present study investigated the effect of roughness to ship resistance and squat in shallow waters. The numerical model presented herein predicted the resistance of the KCS hull with an accuracy of 0.97%, and the sinkage with an error of approximately 2%. A series of case studies were considered to investigate the effect of speed and water depth of the roughness penalty on ship performance. Depth-to-draft ratios of 1.1, 1.2, and 1.3 were investigated, each tested at three speeds.

The frictional and pressure resistance were found to vary significantly when roughness is included. The magnitude of the increase in each case was found to depend on the relative breakdown of the constituent components of resistance. Although both pressure and frictional resistance increase, the former does so at a greater rate than the latter. Specifically, when the depth-to-draft ratio was 1.1 and F_h =0.44, the pressure resistance was predicted to account for approximately 47.8% of the total resistance in the smooth hull case and 51.4% in the rough hull case. In other words, the relative importance of friction diminished across all case studies when roughness was introduced.

The main aim of the study presented in this paper is to investigate a possible roughness dependence of sinkage and trim. The results presented revealed that sinkage is essentially independent of roughness. However, trim was found to vary significantly, echoing recent work showing that trim is influenced by viscous effects. That observation was backed up with an example boundary layer distribution at the aft perpendicular of the vessel which showed significant thickening.

The work presented above can be extended by experimental investigation of the roughness effect in extremely shallow conditions. However, the authors believe that the next stage in this line of research should be an investigation into the roughness effect of the seabed. Specifically, efforts should be directed at quantifying the boundary layer formed on the seabed due to the proximity of an advancing vessel. When testing ship hulls in shallow water using towing tanks, the tank bottom will certainly have some roughness. That effect has yet to be quantified and may go some way to explaining the widespread discrepancy observed by numerous researchers when attempting to predict the trim of a vessel in shallow waters.

Acknowledgements

Results were obtained using the ARCHIE-WeSt High-Performance Computer (www.archie-west.ac.uk) based at the University of Strathclyde. All data underpinning this publication are openly available from the University of Strathclyde KnowledgeBase at https://doi.org/10.15129/2cb92e93-fdd8-44cb-aef1-75fd986f7ed4.

The research presented in this paper was carried out as part of the EU funded H2020 project, VENTuRE (grant no. 856887). The present work was also supported by Inha University Research Grant. This study has been supported by the Croatian Science Foundation under project IP-2020-02-8568.

References

Andersson, J., Oliveira, D.R., Yeginbayeva, I., Leer-Andersen, M., Bensow, R.E., 2020. Review and comparison of methods to model ship hull roughness. Appl. Ocean Res. 99, 102119. https://doi.org/10.1016/j.apor.2020.102119

ASME (American Society of Mechanical Engineers), 2009. Standard for Verification and Validation in Computational Fluid Dynamics and Heat Transfer - ASME V&V 20-2009, ASME International.

Bechthold, J., Kastens, M., 2020. Robustness and quality of squat predictions in extreme shallow water conditions based on RANS-calculations. Ocean Eng. 197, 106780. https://doi.org/10.1016/j.oceaneng.2019.106780

Beck, R.F., Newman, J.N., Tuck, E.O., 1975. Hydrodynamic forces on ships in dredged channels. J. Sh. Res. 19, 166–171.

Benham, G.P., Bendimerad, R., Benzaquen, M., Clanet, C., 2020. Hysteretic wave drag in shallow water. Phys. Rev. Fluids 5, 64803. https://doi.org/10.1103/physrevfluids.5.064803

Burmester, S., Vaz, G., el Moctar, O., 2020. Towards credible CFD simulations for floating offshore wind turbines. Ocean Eng. 209, 107237. https://doi.org/10.1016/j.oceaneng.2020.107237

Campbell, R., Terziev, M., Tezdogan, T., Incecik, A., 2022. Computational fluid dynamics predictions of draught and trim variations on ship resistance in confined waters. Appl. Ocean Res. 126, 103301. https://doi.org/10.1016/j.apor.2022.103301

Caplier, C., Rousseaux, G., Calluaud, D., David, L., 2016. Energy distribution in shallow water ship wakes from a spectral analysis of the wave field. Phys. Fluids 28. https://doi.org/10.1063/1.4964923

Celik, I.B., Ghia, U., Roache, P.J., Freitas, C.., 2008. Procedure for Estimation and Reporting of Uncertainty Due to Discretization in CFD Applications. J. Fluids Eng. 130, 078001. https://doi.org/10.1115/1.2960953

Chen, X.N., 2013. Study of one-dimensional ship squat theories. Chinese J. Hydrodyn. 28, 399–407. https://doi.org/10.3969/j.issn1000-4874.2013.04.004

Chillcce, G., Moctar, O., 2022. Viscous effects on squat. Appl. Ocean Res. 125, 103252. https://doi.org/10.1016/j.apor.2022.103252

Demirel, Y.K., Khorasanchi, M., Turan, O., Incecik, A., Schultz, M.P., 2014. A CFD model for the frictional resistance prediction of antifouling coatings. Ocean Eng. 89, 21–31. https://doi.org/10.1016/j.oceaneng.2014.07.017

Demirel, Y.K., Turan, O., Incecik, A., 2017a. Predicting the effect of biofouling on ship resistance using CFD. Appl. Ocean Res. 62, 100–118. https://doi.org/10.1016/j.apor.2016.12.003

Demirel, Y.K., Uzun, D., Zhang, Y., Fang, H.C., Day, A.H., Turan, O., 2017b. Effect of barnacle fouling on ship resistance and powering. Biofouling 33, 819–834. https://doi.org/10.1080/08927014.2017.1373279

Elsherbiny, K., Terziev, M., Tezdogan, T., Incecik, A., Kotb, M., 2019. Numerical and experimental study on hydrodynamic performance of ships advancing through different canals. Ocean Eng. 106696. https://doi.org/10.1016/j.oceaneng.2019.106696

Farkas, A., Degiuli, N., Martić, I., 2020a. An investigation into the effect of hard fouling on the ship resistance using CFD. Appl. Ocean Res. 100. https://doi.org/10.1016/j.apor.2020.102205

Farkas, A., Degiuli, N., Martić, I., 2018. Towards the prediction of the effect of biofilm on the ship resistance using CFD. Ocean Eng. 167, 169–186. https://doi.org/10.1016/j.oceaneng.2018.08.055

Farkas, A., Song, S., Degiuli, N., Martić, I., Demirel, Y.K., 2020b. Impact of biofilm on the ship propulsion characteristics and the speed reduction. Ocean Eng. 199. https://doi.org/10.1016/j.oceaneng.2020.107033

García, S., Trueba, A., Boullosa-Falces, D., Islam, H., Guedes Soares, C., 2020. Predicting ship frictional resistance due to biofouling using Reynolds-averaged Navier-Stokes simulations. Appl. Ocean Res. 101. https://doi.org/10.1016/j.apor.2020.102203

Gourlay, T., 2014. ShallowFlow: A Program to Model Ship Hydrodynamics in Shallow Water, in: OMAE 2014. p. 8. https://doi.org/10.1115/OMAE2014-23291

Gourlay, T., 2008. Slender-body methods for predicting ship squat. Ocean Eng. 35, 191–200. https://doi.org/10.1016/j.oceaneng.2007.09.001

Gourlay, T., 2006. Flow beneath a ship at small underkeel clearance. J. Sh. Res. 50, 250–258.

Gourlay, T., Ha, J.H., Mucha, P., Uliczka, K., 2015. Sinkage and Trim of Modern Container Ships in Shallow Water. Coast Ports 2015 1–8.

Gourlay, T., Tuck, E.O., 2001. The maximum sinkage of a ship. J. Sh. Res. 45, 50–58.

Grigson, C., 1992. Drag losses of new ships caused by hull finish. J. Sh. Res. 36, 182–

196. https://doi.org/10.5957/jsr.1992.36.2.182

Havelock, T., 1908. The Propagation of Groups of Waves in Dispersive Media, with Aplication to Waves on Water produced by a Travelling Disturbance 422–451. https://doi.org/10.1098/rspa.1933.0074

Havelock, T.H., 1921. The Effect of Shallow Water on Wave Resistance, in: Proceedings of the Royal Society of London. Series A, Containing Papers of a Mathematical and Physical Character. pp. 499–505.

Inui, T., 1954. Wave-Making Resistance in Shallow Sea and in Restricted Water, with Special Reference to its Discontinuities. J. Zosen Kiokai 76, 1–10.

ITTC, 2014. ITTC – Recommended Procedures and Guidelines - Practical guidelines for ship CFD applications. 7.5-03-02-03 (Revision 01). ITTC – Recomm. Proced. Guidel. 19.

ITTC, 2008. Uncertainty Analysis in CFD Verification and Validation Methodology and Procedures. 25th ITTC 2008, Resist. Comm. 12.

Johnson, J.W., 1957. Ship Waves in Navigation Channels. Coast. Eng. Proc. 1, 40. https://doi.org/10.9753/icce.v6.40

Lataire, E., Vantorre, M., Delefortrie, G., 2012. A prediction method for squat in restricted and unrestricted rectangular fairways. Ocean Eng. 55, 71–80. https://doi.org/10.1016/j.oceaneng.2012.07.009

Lazauskas, L. V, 2009. Resistance, Wave-Making and Wave-Decay of Thin Ships, with Emphasis on the Effects of Viscosity. University of Adelaide.

Mctaggart, K., 2018. Ship squat prediction using a potential fl ow Rankine source method. Ocean Eng. 148, 234–246. https://doi.org/10.1016/j.oceaneng.2017.10.016

Menter, F.R., 1994. Two-equation eddy-viscosity turbulence models for engineering applications. AIAA J. 32, 1598–1605. https://doi.org/10.2514/3.12149

Mikkelsen, H., Walther, J.H., 2020. Effect of roughness in full-scale validation of a CFD model of self-propelled ships. Appl. Ocean Res. 99, 102162. https://doi.org/10.1016/j.apor.2020.102162

Mucha, P., Deng, G., Gourlay, T., El Moctar, O., 2016. Validation Studies on Numerical Prediction of Ship Squat and Resistance in Shallow Water. Proc. 4th Int. Conf. Sh. Manoeuvring Shallow Confin. Water (MASHCON), 23 - 25 May 2016, Hamburg, Ger. 0, 122–133. https://doi.org/10.18451/978-3-939230-38-0

Mucha, P., el Moctar, B., 2014. Numerical Prediction of Resistance and Squat for a Containership in Shallow Water, in: Bensow, R.E. (Ed.), Proceedings of the 17th Numerical Towing Tank Symposium. Marstrand, Sweden.

Peric, M., 2019. White paper: Full-scale simulation for marine design. Siemens White Pap.

PIANC, 2014. Report 121 - 2014.

Ravenna, R., Song, S., Ship, W., Sant, T., De Marco Muscat-Fenech, C., Tezdogan, T., Demirel, Y.K., 2022. CFD analysis of the effect of heterogeneous hull roughness on ship resistance. Ocean Eng. August. https://doi.org/10.3390/jmse9020202

Regitasyali, S., Hakim, M.L., Utama, I.K.A.P., 2021. CFD analysis of the increase in ship resistance due to biofouling growth represented by roughness length scale, in: IOP Conference Series: Materials Science and Engineering. https://doi.org/10.1088/1757-899x/1052/1/012034

Roache, P.J., 2016. Verification and Validation in Fluids Engineering: Some Current Issues. J. Fluids Eng. 138, 101205. https://doi.org/10.1115/1.4033979

Schultz, M.P., 2004. Frictional resistance of antifouling coating systems. J. Fluids Eng. Trans. ASME 126, 1039–1047. https://doi.org/10.1115/1.1845552

Schultz, M.P., Bendick, J.A., Holm, E.R., Hertel, W.M., 2011. Economic impact of biofouling on a naval surface ship. Biofouling 27, 87–98. https://doi.org/10.1080/08927014.2010.542809

Schultz, M.P., Flack, K.A., 2007. The rough-wall turbulent boundary layer from the hydraulically smooth to the fully rough regime. J. Fluid Mech. 580, 381–405. https://doi.org/10.1017/S0022112007005502

Seok, J., Park, J.C., 2020. A fundamental study on measurement of hull roughness. Brodogradnja 71, 59–69. https://doi.org/10.21278/brod71104

Shevchuk, I., Böttner, C.U., Kornev, N., 2016. Numerical Analysis of the Flow in the Gap Between the Ship Hull and the Fairway Bottom in Extremely Shallow Water. Proc. 4th Int. Conf. Sh. Manoeuvring Shallow Confin. Water (MASHCON), 23 - 25 May 2016, Hamburg, Ger. 0, 37–42. https://doi.org/10.18451/978-3-939230-38-0

Song, S., Dai, S., Demirel, Y.K., Atlar, M., Day, S., Turan, O., 2021. Experimental and theoretical study of the effect of hull roughness on ship resistance. J. Sh. Res. 65, 62–71. https://doi.org/10.5957/JOSR.07190040

Song, S., Demirel, Y.K., Atlar, M., 2019. An investigation into the effect of biofouling on the ship hydrodynamic characteristics using CFD. Ocean Eng. 175, 122–137. https://doi.org/10.1016/j.oceaneng.2019.01.056

Song, S., Demirel, Y.K., Atlar, M., Dai, S., Day, S., Turan, O., 2020a. Validation of the CFD approach for modelling roughness effect on ship resistance. Ocean Eng. 200, 107029. https://doi.org/10.1016/j.oceaneng.2020.107029

Song, S., Demirel, Y.K., De Marco Muscat-Fenech, C., Tezdogan, T., Atlar, M., 2020b. Fouling effect on the resistance of different ship types. Ocean Eng. 216, 107736. https://doi.org/10.1016/j.oceaneng.2020.107736

Terziev, M., Tezdogan, T., Demirel, Y.K., Villa, D., Mizzi, S., Incecik, A., 2021a. Exploring the effects of speed and scale on a ship's form factor using CFD. Int. J. Nav. Archit. Ocean Eng. 13, 147–162. https://doi.org/10.1016/j.ijnaoe.2020.12.002

Terziev, M., Tezdogan, T., Incecik, A., 2022. Scale effects and full-scale ship hydrodynamics: A review. Ocean Eng. 245, 110496. https://doi.org/10.1016/j.oceaneng.2021.110496

Terziev, M., Tezdogan, T., Incecik, A., 2021b. A numerical assessment of the scale effects of a ship advancing through restricted waters. Ocean Eng. 229, 108972. https://doi.org/10.1016/j.oceaneng.2021.108972

Terziev, M., Tezdogan, T., Incecik, A., 2019. Application of eddy-viscosity turbulence models to problems in ship hydrodynamics. Ships Offshore Struct. 1–24. https://doi.org/10.1080/17445302.2019.1661625

Terziev, M., Tezdogan, T., Oguz, E., Gourlay, T., Demirel, Y.K., Incecik, A., 2018. Numerical investigation of the behaviour and performance of ships advancing through restricted shallow waters. J. Fluids Struct. 76, 185–215. https://doi.org/10.1016/j.jfluidstructs.2017.10.003

Terziev, M., Zhao, G., Tezdogan, T., Yuan, Z., Incecik, A., 2020. Virtual Replica of a Towing Tank Experiment to Determine the Kelvin Half-Angle of a Ship in Restricted Water. J. Mar. Sci. Eng. 8, 1–24. https://doi.org/10.3390/jmse8040258

Tuck, E.O., 1978. Hydrodynamic Problems of Ships in Restricted Waters. Annu. Rev. Fluid Mech. 10, 33–46.

Tuck, E.O., 1967. Sinkage and Trim in Shallow Water of Finite Width. Schiffstechnik 14, 92–94.

Tuck, E.O., 1966. Shallow-Water Flows Past Slender Bodies. J. Fluid Mech. 26, 81–95. https://doi.org/10.1017/S0022112066001101

Zeng, Q., Hekkenberg, R., Thill, C., 2019a. On the viscous resistance of ships sailing in shallow water. Ocean Eng. 190, 106434. https://doi.org/10.1016/j.oceaneng.2019.106434

Zeng, Q., Hekkenberg, R., Thill, C., 2019b. A study of ship's frictional resistance in extremely shallow water, in: Proceedings of the International Conference on Offshore Mechanics and Arctic Engineering - OMAE. pp. 1–11. https://doi.org/10.1115/OMAE2019-95076

Zeng, Q., Thill, C., Hekkenberg, R., Rotteveel, E., 2018. A modification of the ITTC57

correlation line for shallow water. J. Mar. Sci. Technol. 0, 0. https://doi.org/10.1007/s00773-018-0578-7